8.1 CORRECTED TOGA-COARE SOUNDING HUMIDITY DATA: IMPACT ON CLIMATE AND CONVECTION OVER THE WARM POOL

Richard H. Johnson* and Paul E. Ciesielski
Colorado State University, Fort Collins, Colorado

1. INTRODUCTION

Shortly after the field phase of the 1992-93 Tropical Ocean Global Atmosphere (TOGA) Coupled Ocean-Atmosphere Response Experiment (COARE) it became apparent that the sounding systems used in the COARE Large Scale Array (LSA), a combination of Vaisala- and VIZ-manufactured systems, exhibited a variety of humidity errors. Lucas and Zipser (2000) noted unrealistically small values of Convective Available Potential Energy (CAPE) at many of the Integrated Sounding System (ISS) sites, where Vaisala-H humidity sensors were used, and concluded that these sensors displayed a dry bias (∼5% in relative humidity) in the lower troposphere. They developed a correction algorithm for the Vaisala humidity data based on independent observations of surface humidity and their differences from sounding-determined mixed-layer mean values. Without the corrections, large horizontal gradients of low-level moisture over regions of nearly uniform sea surface temperature were observed, with CAPE varying by a factor of 2.5 over the COARE Intensive Flux Array (IFA) (Zipser and Johnson 1998). After corrections, a more homogeneous horizontal distribution of humidity over the IFA was achieved.

Recently, Wang et al. (2002) investigated the humidity errors in the Vaisala systems used in COARE and developed a procedure for correcting them. Guichard et al. (2000) studied the impact of the errors for one site (R/V *Moana Wave*) and found that after application of the humidity corrections, the atmosphere exhibited more realistic values of CAPE and convective inhibition (CIN), comparable to those determined from aircraft observations. They also found an important effect of the corrected moisture fields on the surface radiative budget. It is worth emphasizing that these humidity corrections for the Vaisala systems are not unique to the COARE region, but are apply to operational systems used throughout the world.

* *Corresponding author address:* Richard H. Johnson, Department of Atmospheric Science, Colorado State University, Fort Collins, CO 80523-1371; johnson@atmos.colostate.edu

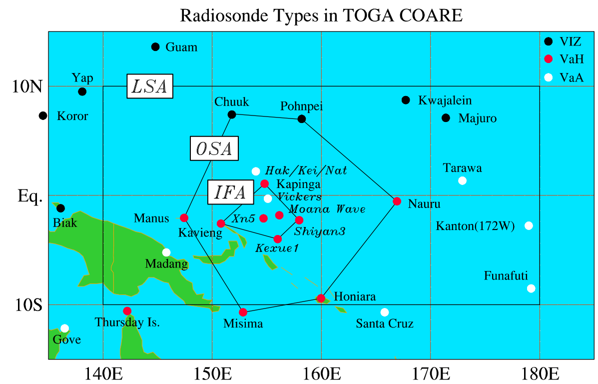

Figure 1: Map showing various types of radiosonde sensors used during TOGA COARE. Also shown are the Large-Scale Array (LSA), the Outer Sounding Array (OSA), and the Intensive Flux Array (IFA). The locations of research vessels (italics) represent their nominal positions. Japanese ships, shown north of the IFA, cruised in and out of the IFA.

In contrast, evidence from the VIZ humidity observations, which were taken at stations in the northern part of the LSA (Fig. 1), revealed a moist bias in the lower troposphere (Johnson and Ciesielski 2000), consistent with earlier findings for VIZ systems elsewhere by Wade and Schwartz (1993).

In this paper we explore humidity biases for COARE soundings in greater detail and over a larger area than in past studies, and examine their impacts on climate and convection over the warm pool. To do so, the humidity corrections of Wang et al. (2002) are applied to all Vaisala sites in and near the COARE LSA and a new correction procedure is developed for the VIZ systems.

2. NATURE OF HUMIDITY CORRECTIONS AND DATA SOURCES

Three types of radiosondes were used during COARE: the Vaisala RS80_H (VaH) and its predecessor the RS80_A (VaA), which have capacative humidity sensors, and the VIZ system which has a resistance-type humidity sensor. The VaH systems, deployed at the ISS sites, were used at the majority of the IFA sites, while the VIZ systems were used primarily at sites around 10°N.

A cooperative study by NCAR Atmospheric Technology Division (ATD) and Vaisala led to the identification of six difference humidity errors. A detailed description of these errors and procedures to correct them can be found in Wang et al. (2002). For temperatures above -20°C, the most serious error was due to chemical contamination of the humidity sensor, a dielectric polymer, by aging packing material. The contamination error reduced the ability of the sensor to absorb water vapor resulting in a dry bias which increased with sonde age and relative humidity (RH). This error is larger in VaH sondes, such that for a one-year old VaH sonde at saturation the RH is about 10% too low. For temperatures below -20°C an error referred to as the temperature dependent (TD) error dominates. Occurring in both VaH and VaA sondes type, this error resulted from approximating the actual non-linear temperature dependence of the humidity sensor by a linear function. The TD error, which is larger in the VaA sondes, increases with decreasing temperature. Applying an algorithm to correct for the six errors, NCAR ATD corrected the humidity data in 8129 sondes at 29 Vaisala sites. After the corrections were made, each sonde was visually inspected and "unreasonable" humidity data values generated by the correction procedure were changed to missing values.

The VIZ sensor was characterized by a low-level (below 750 hPa) moist bias which was considerably larger in the nighttime sondes. The moist bias in the daytime sondes may have been reduced by daytime heating of the VIZ hygristor. In addition to this low-level moist bias, a significant mid-level (700-300 hPa) dry bias relative to the mean Vaisala profiles (Fig. 2) is observed in the VIZ data. It is not known to what extent this dry bias reflects real horizontal variability.

Although the reasons for the biases in the VIZ sensors are still uncertain, NCAR/ATD developed a correction procedure, based on a modified hygristor response curve (suggested by Wade and Schwartz 1993). This procedure, which reduces the low-level moist bias by as much as 4%, was applied to correct 3411 VIZ soundings at 13 sites. As a final check of the correction procedure, the humidity data from each sonde were visually inspected in a skew$-T$ format and obvious glitches were set to missing values. While the current VIZ correction procedure is incomplete, specifically lacking a correction above 700 hPa, its reduction of the lower tropospheric moist bias appears reasonable, and thus useful for our present purpose.

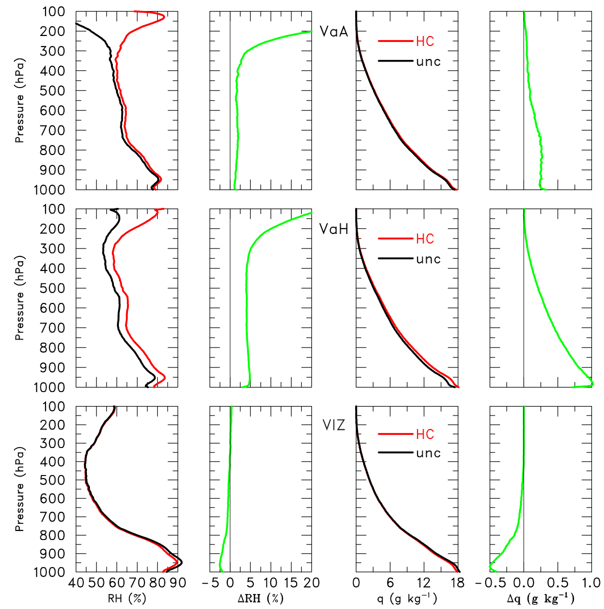

Figure 2: Magnitude of humidity correction (HC) for various sensor types: VaA (top panels), VaH (middle panels), and VIZ (bottom panels). Curves show mean vertical profiles and their difference (Δ = HC value − uncorrected value) for relative humidity with respect to ice (leftmost two panels) and specific humidity (rightmost two panels).

In this study the impacts of the humidity corrections on various analyses are examined relative to an "uncorrected" humidity dataset. The "uncorrected" upper-air dataset was obtained from Joint Office for Science Support (JOSS) TOGA COARE web site. Wang et al. (2002) point out that this earlier version of the upper-air sonde dataset actually contains an erroneous correction for a sensor arm heating (SAH) error. Based on their analyses Wang et al. develop a revised correction procedure for the SAH error. The corrected humidity upper-air Vaisala and VIZ sonde data were obtained from NCAR ATD.[1] For more accurate analysis of atmospheric budgets, a merged dataset of rawinsonde and profiler winds at the ISS sites (Ciesielski et al. 1997) was used in this present study.

For computation of atmospheric budgets, fields of surface evaporation E and sensible heat flux S are based on NCEP reanalysis values adjusted to-

[1]The Vaisala humidity corrected sonde data in their native vertical resolution were made available at JOSS during Spring 2002; due to limitations in the VIZ humidity corrections and pending further analyses, the VIZ humidity-corrected sonde data have not been released to JOSS.

Sonde type	VaA			VaH			VIZ		
Number of sondes	1218			3891			2724		
Parameter	unc	cor	Δ	unc	cor	Δ	unc	cor	Δ
CAPE (J kg^{-1})	921	961	(+40)	822	1272	(+450)	1535	1241	(−294)
CIN (J kg^{-1})	−101	−65	(+36)	−139	−43	(+96)	−20	−22	(−2)
PW (kg m^{-2})	50.5	51.4	(+0.9)	49.1	52.1	(+3.0)	48.4	47.6	(−0.8)
LCL (hPa)	923	925	(+2)	918	930	(+12)	950	944	(−6)
LNB (hPa)	162	157	(-5)	172	157	(−17)	145	155	(+10)

Table 1. Impact of corrected humidity data on convective parameters computed from sondes launched from the sites shown in Fig. 1. Δ refers to the change in a parameter as a result of using the corrected humidity data.

wards an IFA-mean value representing the average of four buoys in or near the IFA (Lin and Johnson 1996). The GMS-4 brightness temperature data used to help distinguish clear and cloudy periods in Section 5 were provided by Dr. Tetsuo Nakazawa.

For comparison to budget-derived rainfall, satellite estimates of rainfall for the COARE domain were obtained from two sources: the CMAP (Climate prediction center Merged Analysis of Precipitation) analysis of Xie and Arkin (1997), and the mixed rainfall algorithm of Curry et al. (1999). The CMAP analysis, available on a monthly basis at 2.5° resolution, represents a merger of rain gauge with a variety of infrared (IR) and microwave satellite estimates. The Curry analysis, at 3-h and 0.5° resolution over the IFA domain, combines visible and IR data from geostationary satellites with microwave rainfall retrievals from polar-orbiting satellites.

3. MAGNITUDE OF THE HUMIDITY CORRECTION

Figure 2 shows the magnitude of the humidity correction for the various sensor types used in the COARE domain in terms of relative humidity (RH, left-hand panels) and specific humidity (q, right-hand panels). These mean profiles were constructed by averaging individual sondes at 5 hPa resolution from all the sites shown in Fig. 1. The number of sondes that entered into the mean for each sensor type are listed in Table 1.

In the VaA sondes, the correction increases the mean RH about 1-2% below 300 hPa with a dramatic increase in the correction above this level to a maximum of over 50% (not shown) near 100 hPa. In terms of specific humidity, the correction moistens the troposphere below 700 hPa about 0.25 g kg^{-1}

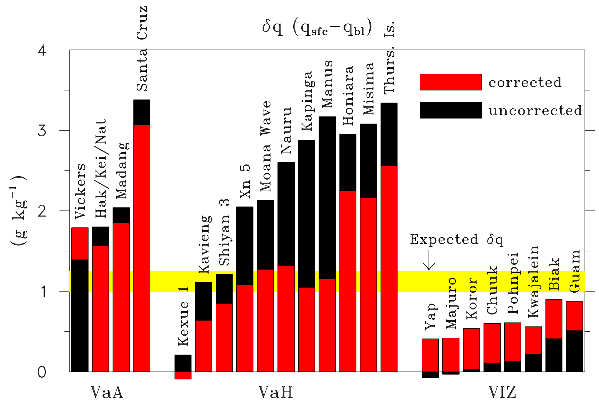

Figure 3: Difference between the surface and boundary layer mean specific humidity, δq, for several of the sounding sites shown in Fig. 1 computed with uncorrected data (top of black bar, except at Yap and Majuro which have a negative uncorrected difference) and humidity corrected (HC) data (top of red bar, except for *Kexue 1* in which case the corrected data results in a negative δq). The horizontal yellow bar denotes the expected range for δq in the warm pool region. Sites are grouped according to sonde-sensor type: VaA, VaH and VIZ (from left to right).

with a gradual decrease above this level. In the VaH sondes, the humidity-corrected (HC) data increases the mean RH about 5% below 300 hPa. Above this level the correction increases to a maximum of about 20% near 100 hPa. In terms of specific humidity the correction moistens the boundary layer about 1 g kg^{-1} with a gradual decrease in the correction with height. In the VIZ sondes, the correction has little or no impact above 700 hPa. Below this level the correction decreases mean RH from 2-3% which translates into a 0.5 g kg^{-1} decrease in specific humidity at 950 hPa.

Having examined how the correction data affects humidity as a function of sensor type, we now focus on its impact in the boundary layer at individual sites. Figure 3 shows the mean specific humidity difference (δq) between the surface and boundary layer computed from sondes launched during the COARE IOP. The surface q value represents an observation from a surface-based sensor independent of the sonde, while the boundary layer value is the mean q averaged from the first point above the surface up to and including the 960 hPa level. This analysis is shown only for sites from Fig. 1 which had at least 100 soundings of good quality data in both the humidity corrected and uncorrected dataset[2]. Re-

[2]At the time that the "uncorrected" sonde data were released, many of the humidity errors in the data were still unknown such that data containing these errors were

sults from the three Japanese ships (R/V *Hakuho-Naru, Keifu Maru, Natsushima*) which collectively launched 170 sondes in the vicinity of the IFA are considered together. In Fig. 3 the top of the black (red) bar represents the mean δq computed with uncorrected (corrected) humidity data. The only exception to this is for R/V *Kexue 1* in which the bottom of the red bar represents the corrected gradient (i.e., the corrected q gradient is negative).

Evidence from low-level COARE aircraft measurements and Monin-Obukhov similarity theory indicate that δq should be $\sim$1.0–1.25 g kg^{-1} over the warm pool region (Zipser and Johnson 1998). While only a few sites exhibit this magnitude of δq with uncorrected data, the δq's computed with the HC data are in much better agreement with this expected value. In general, the correction acts to dry out the boundary layer of the VIZ sites (i.e., δq increases), and moistens the boundary layer of the Vaisala sites (i.e., δq decreases). The exception to this is with the R/V *Vickers*, a VaA site which showed a dry correction. At this site, young sonde age combined with careful ground check corrections prior to launch yielded an original dataset that was quite accurate, and as such, humidity corrections were unnecessary. Also, the main source of humidity error at R/V *Kexue 1* was different in nature[3] from those at the other Vaisala sites resulting in a low-level moist bias at this site. The correction procedure, which was not designed to handle a moist bias at a Vaisala site, had an adverse effect upon the correction of humidity at this site. For consistency NCAR ATD applied a similar correction procedure to all Vaisala sites. However, for the reasons stated above, uncorrected humidity data from the *Vickers* and *Kexue 1* are judged to be of better quality, so that the "corrected" data from these two sites are not considered further in this study.

Of the six IFA sounding sites that were present for the majority of the IOP[4] all have a corrected δq near or < 1.0 g kg^{-1}, except for the *Moana Wave* which has $\delta q = 1.3$ g kg^{-1} (Fig. 3). In studying the mixed layer properties at four IFA sites (*Shiyan 3*, *Xn 5*, *Moana Wave*, Kapinga) with the HC dataset, Johnson et al. (2001) found that the difference between the mean lifting condensation level (LCL) and the mean mixed layer top was $\sim$170 m at three of the sites, the exception being the *Moana Wave* where the difference was 240 m. Since a drier boundary layer leads to a higher LCL, Johnson et al. suggested that the humidity at the *Moana Wave* was slightly undercorrected, which is consistent with its larger corrected δq in Fig. 3. Finally we note, that four Vaisala sites (Honiara, Misima, Thursday Island and Santa Cruz) have large δq's (> 2 g kg^{-1}) even with HC data. While the reason for these larger δq's is uncertain, it is worth noting that these four sites are all located on larger islands and are geographically grouped along 10°S in a region of cooler SSTs (cf Fig. 5 from Lin and Johnson 1996).

4. IMPACTS ON DIAGNOSED PROPERTIES OF CONVECTION

Table 1 shows the impact of using the HC data on various convective parameters. These computations were done for all soundings which had good quality data over the entire depth of the troposphere and for all sites shown in Fig. 1. In this table and throughout the rest of this paper, the symbol Δ signifies the change in a quantity resulting from use of the HC data. Convective Available Potential Energy (CAPE) and Convective Inhibition (CIN) were calculated assuming pseudo-adiabatic ascent using mean thermodynamic conditions in the lowest 50 hPa. In the VaH sondes, use of the HC data results in large changes in the mean convective parameters: CAPE increases 450 J kg^{-1}, CIN deceases 96 J kg^{-1}, precipitable water (PW) increases by 3 kg m^{-2}, the LCL lowers 12 hPa and the level of neutral buoyancy (LNB) rises 22 hPa. The changes in these parameters in the VaA sondes are in same sense but considerably smaller in magnitude, consistent with the smaller humidity changes noted in Figs. 2 and 3. For the VIZ sondes, use of the humidity corrections results in modest changes in the convective parameters but in an opposite sense. The smaller values of PW in the VIZ sondes compared to the Vaisala sondes reflects the mid-level dryness in the VIZ data.

Comparison of the mean CAPE values at the VIZ and VaH sites in Table 1, show much better agreement when computed with the HC data, both being around 1250 J kg^{-1}. This value, being representative of sondes launched in both convectively active and suppressed periods, seems reasonable when compared with the mean CAPE value of 1471 J kg^{-1} found by LeMone et al. (1998) based on aircraft measurements in the vicinity of twenty convective systems.

On the basis of CAPE and CIN values in Table 1

typically flagged as being of good quality.

[3]The sondes on the *Kexue 1* were stored in a very cold, air conditioned room such that condensation formed on humidity sensor when the sondes were taken from the room resulting in the observed low-level moist bias.

[4]*Kexue 1*, *Shiyan 3*, *Xn 5*, *Moana Wave*, Kavieng, and Kapinga

computed with uncorrected Vaisala data, we concur with the assessment of Guichard et al. (2000) that "one might erroneously conclude that it is difficult to trigger deep convection over the region" of the warm pool near the IFA. However when the humidity corrections are considered in the Vaisala sondes, we observe an atmosphere "typically near a threshold where convection is easily initiated or least maintained" (Guichard et al. 2000). On the other hand, the high CAPE and low CIN values observed in the uncorrected VIZ data near 10°N might lead one to mistakenly conclude that the atmospheric state in the vicinity of the VIZ sites is one with almost no convective inhibition and primed for vigorous convective development, yet deep convection was much reduced near the VIZ sites in comparison with that in the IFA (Fig. 7, later).

Changes in CAPE and CIN at individual sites due to the HC data are shown in Fig. 4. As one might expect, the magnitude of changes in these parameters at individual sites generally follows the magnitude of the boundary layer moisture change (δq) depicted in Fig. 3. While most sites show only modest changes in CAPE and CIN due to the humidity corrections, the changes at a few sites are quite large. For example, at Nauru and Kapinga the mean CAPE increases over 800 J kg^{-1}, while at Kapinga and Honiara the CIN decreases over 200 J kg^{-1}. These site-to-site differences in the convective parameters changes suggest that the geographical distribution of convection could be significantly different when modeled with the HC dataset.

To further explore the impact the humidity corrections on convection, we utilize the buoyancy-sorting cloud model of Raymond and Blyth (1992). This model is based on the premise that entrainment and mixing in clouds occurs as a random, highly episodic process. In this model, a parcel representing the mean properties of the 1000-950 hPa layer ascends through the troposphere up to the LNB. At each 5 hPa level the parcel mixes with environmental air with different mixing fractions ranging from 0.1 to 0.9. These diluted parcels then ascend or descend to their nearest level of neutral buoyancy with no overshooting allowed. For the results to be shown here, we assume that as the parcel ascends and water condenses, it can hold a maximum of 3 g kg^{-1} of liquid water. Above this threshold, which represents a mid-range value used in GATE (Global Atmospheric Research Program Atlantic Tropical Experiment) simulations (Ferrier and Houze 1989), water falls out as precipitation.

The model was applied to individual sondes (both humidity-corrected and uncorrected) from

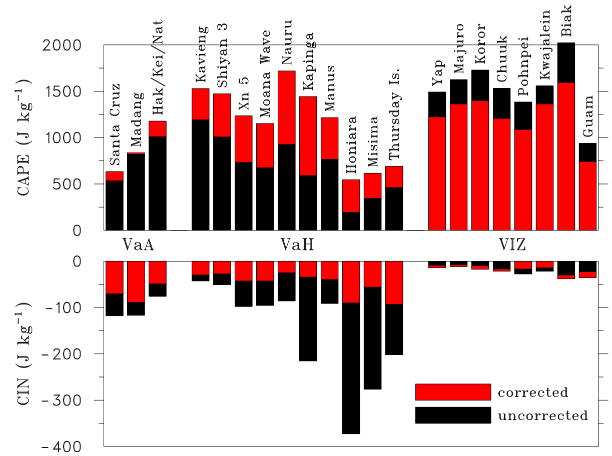

Figure 4: Top panel shows mean values of CAPE at several sounding sites computed with humidity corrected data (top of red bar) and uncorrected data (top of black bar). Bottom panel shows mean values of CIN computed with humidity corrected data (bottom of red bar) and uncorrected data (bottom of black bar). Sites are grouped according to sonde-sensor type: VaA, VaH and VIZ (from left to right).

seven sites for each sensor type. Model results from the individual sondes, which were required to have good thermodynamic data through the depth of the troposphere, were then averaged into mean profiles for each sensor type. The VIZ sites (2351 sondes) were between 7° and 13°N; the seven VaH sites (1979 sondes) were within 3° of the equator (see Fig. 1). In this manner, the mean profiles are representative not only of a sensor type but also of a geographical region. Unfortunately a smaller regional grouping for the VaA sites was not possible, so that the seven VaA sites (795 sondes) used were from within the LSA domain. Results from the model for the various sensor types are shown in Fig. 5 in terms of mean vertical profiles of detrainment probability and convective mass flux. The results in the left-hand panels are for the case where no ice effects are included, whereas those on the right allow for ice formation which enhances parcel buoyancy.

The small humidity increases in the corrected VaA sondes, depicted in Figs. 2 and 3, have little or no impact on detrainment and convective mass flux profiles. In contrast, the humidity-corrected VaH data have a significant impact on these fields with less detrainment below 250 hPa and nearly twice the frequency of outflow layers above this level. In the no ice case, there is a secondary peak in outflow layers observed near 400 hPa, presumably related to a layer of enhanced stability near the 0°C level (Johnson et al. 1996, Zuidema 1998). When

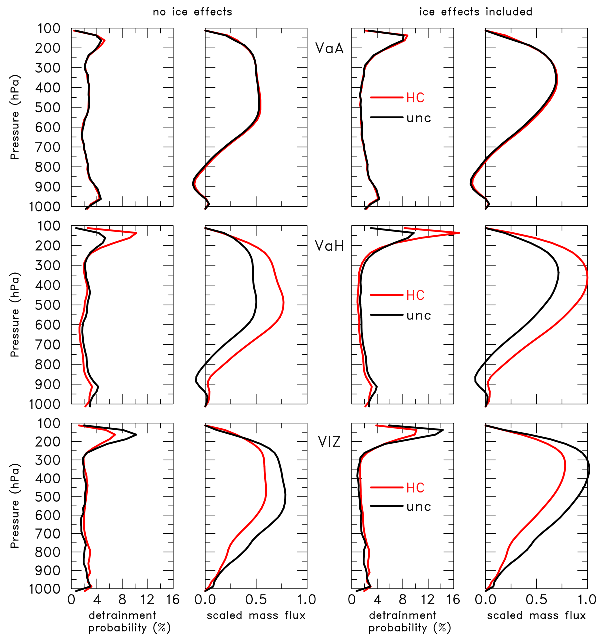

Figure 5: Vertical mean profiles of detrainment probability and scaled convective mass flux from the Raymond-Blyth buoyancy-sorting cloud model computed with humidity corrected data (red curve) and uncorrected data (black curve) for the different sonde-sensor types: VaA (top panels), VaH (middle panels), and VIZ (bottom panels). Left-most two panels show results with no ice-effects, while right-most two panels show results where ice formation is allowed. The mass flux profiles have been normalized by the largest mass flux value.

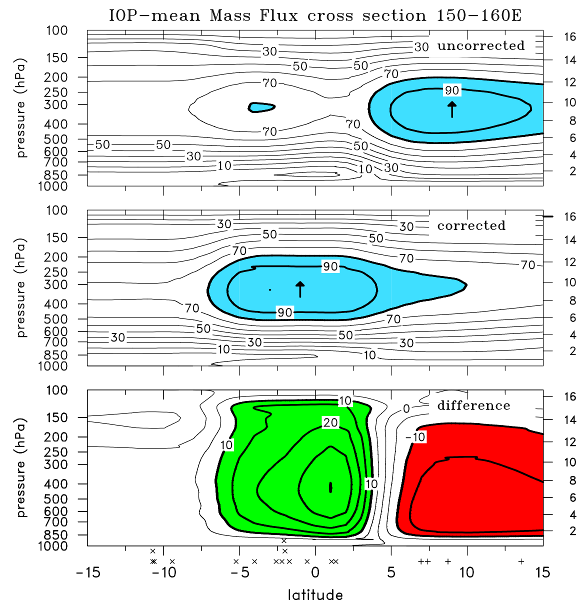

Figure 6: IOP-mean zonally averaged convective mass flux (normalized by maximum value) between 150° and 160°E computed with uncorrected data (top panel), corrected data (middle panel) and their difference (bottom panel). In the top two panels values greater than 80 units are shaded. In the bottom panel differences greater than 10 units are shaded green and less than −10 units are shaded red. Symbols at the base of the bottom panel indicate the latitudes of Vaisala (×) and VIZ (+) sites used in creating this analysis.

ice effects are included, this secondary detrainment is no longer present as the additional latent heating due to freezing and deposition enhances buoyancy allowing more parcels to detrain at higher levels. These changes in detrainment due to use of HC data translate into an ∼30% increase in the mean convective mass flux in the 500-300 hPa layer. Using the humidity corrected VIZ sondes results in trends in these fields that are in opposite sense, that is, a reduction in the frequency of upper-level outflow layers corresponding to an ∼15% reduction in the mean convective mass flux in the 500-300 hPa layer. Based on the IOP-mean mass flux profiles at individual sites, Fig. 6 shows a longitudinal cross section of mass flux with corrected and uncorrected data. This analysis shows that the peak in the IOP-mean mass flux shifts from about 8°N with the uncorrected data to just south of the equator with HC data which is more consistent with the observed rainfall pattern (see CMAP rainfall analysis in Fig. 7) for this period. Hence these results show that the HC data have a significant impact on the intensity and distribution of convection.

To further explore this effect, a cross section of the IOP-mean RH has been prepared for the longitude belt from 150°E to 160°E where the sonde data coverage over the warm pool is most plentiful (Fig. 7). The top panel shows the RH cross section computed with uncorrected data and the bottom panel with HC data. Also shown in the bottom panel are the latitudinal locations of the sounding sites which influenced this analysis where sites with a Vaisala sensor are indicated with a "×" symbol and sites with VIZ sensor have a "+" symbol. In the uncorrected cross section, the boundary layer humidity shows a maximum over 90% in the vicinity of the VIZ sites centered around 10°N. Use of the HC data leads to a more horizontally homogeneous boundary layer moisture pattern with a maximum of 85% at nearly all latitudes north of 5°S. Also, the mid- and upper levels are moistened at the latitudes of the Vaisala sites (south of 2°N), while the mid-level dryness is readily apparent in both cross sections at the latitudes of the VIZ sites. Using a two-dimensional cloud model to study western Pacific squall lines, Lucas et al. (2000) found that increasing the moisture content above the boundary layer,

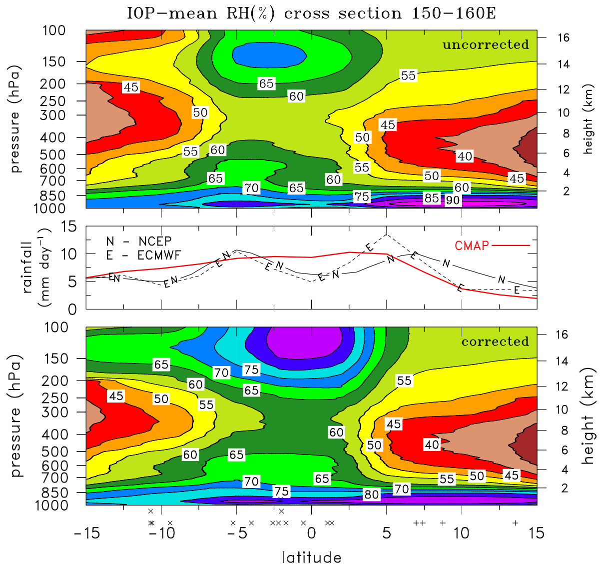

Figure 7: IOP-mean zonally averaged relative humidity between 150° and 160°E computed with uncorrected data (top panel) and HC data (bottom panel). Symbols at the base of the bottom panel indicate the latitudes of Vaisala (×) and VIZ (+) sites used in creating this analysis. The middle panel shows the IOP-mean zonally averaged rainfall rate for the same longitude band for the NCEP and ECMWF reanalyses and the CMAP rainfall product (red curve). Relative humidity was computed with respect to ice for temperatures less than 0°C.

particularly up to 3 km, was favorable for strengthening squall lines. Thus the moisture corrections in the boundary layer, as well as above it (as depicted in Figs. 2 and 7), will likely affect simulations of convection.

The middle panel of Fig. 7 shows the IOP-mean rainfall averaged over the same longitude band from three sources: the NCEP and ECMWF reanalysis products which are based on uncorrected humidity data, and the satellite-based CMAP analysis. While the CMAP analysis shows a broad maximum with a peak around 2.5°N, the reanalysis products have two peaks - one at 5°S and the other at 5–7.5°N with a relative minimum over the latitudes of the IFA (centered around the equator). The excessive rainfall north of ∼5°N and the deficit to the south in the reanalysis products follows the moisture biases depicted in the uncorrected humidity cross-section. It would appear that the convective parameterizations used in the reanalysis models have translated the humidity biases into an erroneous rainfall pattern (Johnson and Ciesielski 2000). Interestingly, the changes in the convective mass fluxes distribution due to the HC data depicted in Fig. 6 are of the right order to bring the reanalysis rainfall amounts into good agreement with the CMAP rainfall estimate. This suggests that the ECMWF and NCEP analysis products for the COARE period would benefit from a new reanalysis with the HC data.

5. IMPACTS ON RAINFALL AND RADIATIVE HEATING RATE ESTIMATES

In this section we examine impacts of using the HC sonde data on diagnosed rainfall and radiative heating rates from atmospheric heat and moisture budgets. Sensitivity test designed to gauge impact of the HC data will focus primarily on the IFA region where measurements were most abundant and the analyses are most frequently used. To facilitate this testing, objective analysis of the horizontal wind components u and v, temperature T, specific humidity q (both corrected and uncorrected), and geopotential height z at 1° horizontal resolution, 25-hPa vertical resolution were produced over the area of the LSA (140–180°E, 10°S–10°N). These analyses were computed every 6 hours for the COARE IOP using the multiquadric interpolation scheme of Nuss and Titley (1994). To assist the analysis in data sparse regions, ECMWF reanalysis values were used along 15°N and along 180°E north of the equator at 5° intervals. The extraction of reliable fields of divergence from sparce sounding networks such as COARE presents a formidable challenge (e.g., Ooyama 1987, Zhang and Lin 1997)

In earlier versions of our gridded analyses, dipoles in the vertically-averaged horizontal divergence field were observed in the vicinity of the sounding stations. Recently, Haertel (2002) concluded that these features were spurious in nature and generated by the analysis scheme. To remove this spurious divergence, a correction algorithm was developed (Haertel 2002) and has applied here to the adjust the horizontal winds and divergence. Additional details of the objective analysis procedure and computation of the omega field can be found in Johnson and Ciesielski (2000).

Following Yanai et al. (1973), vertical integration of the conservation laws of heat and moisture yield

$$< Q_1 > \; = \; < Q_R > + LP + S \;,^5 \qquad (1)$$

$$< Q_2 > \; = \; L(P - E) \;, \qquad (2)$$

[5] The form of this equation ignores a term involving the vertical integral of the latent heat of fusion times deposition minus sublimation (Gallus and Johnson 1991).

where the apparent heat source Q_1, is defined as $c_p[(\partial\bar{T}/\partial t + \bar{\mathbf{v}}\cdot\nabla\bar{T} + (p/p_0)^\kappa\bar{\omega}\partial\bar{\theta}/\partial p)]$, and the apparent moisture sink Q_2, is defined as $-L(\partial\bar{q}/\partial t + \bar{\mathbf{v}}\cdot\nabla\bar{q} + \bar{\omega}\partial\bar{q}/\partial p)$ where where $\kappa = R/c_p$, R is the gas constant, and c_p the specific heat at constant pressure for moist air, L the temperature-dependent latent heat of vaporization, $< Q_R >$ the net radiative heating rate, P the precipitation rate, overbar denotes a horizontal average, $< \quad > \equiv 1/g\int_{p_T}^{p_s}(\quad)dp$, p_T is the tropopause pressure and p_s the surface pressure. Combining $(1-2)$ yields:

$$< Q_R > = < Q_1 > - < Q_2 > - S - LE \ . \qquad (3)$$

Our approach is to first compute the quantities of Q_1 and Q_2 with our gridded dataset, then compute precipitation P and net-radiative heating $< Q_R >$ as budget residuals from (2) and (3), respectively.

Figure 8 shows the IFA-IOP-mean vertical profiles for apparent heating, apparent moistening, and specific humidity where the latter two fields were computed with both the uncorrected and corrected humidity data. Using the HC data produces an increase in Q_2, most notably at lower levels, where the apparent moistening below 925 hPa is substantially reduced. This increase in Q_2 can be understood by noting that the major contribution to the apparent drying field (above the surface) comes from the vertical advection term, $-L(\bar{\omega}\partial\bar{q}/\partial p)$. Thus, the steeper vertical gradient of q in the HC data results directly in the increased apparent drying rate seen here. Near and at the surface, corrections to the horizontal advection of q account for the increase in Q_2. This increase in Q_2 has important implications for the budget-derived quantities since as seen in (2) and (3), precipitation and net-radiative cooling increase as the of the vertical integral of Q_2 increases.

The IFA-mean time series of precipitation and net-radiative heating (computed with both corrected and uncorrected humidity data) for the COARE IOP are shown in Fig. 9. Use of the HC data results in a small increase in rain rate over during much of the IOP. Compared to the uncorrected rainfall time series, the HC rainfall shows a higher correlation to an estimate based on the mixed satellite algorithm of Curry et al. (1999) increasing from 0.72 to 0.75 for six-hourly values (or 0.79 to 0.84 if one considers the 5-day running mean rainfall). The changes in the net-radiative time series are more dramatic with substantially more cooling over extended periods. Most notably, the period of strong radiative warming near the end of December, and coincident with a strong westerly wind burst, is nearly eliminated when computed with HC data.

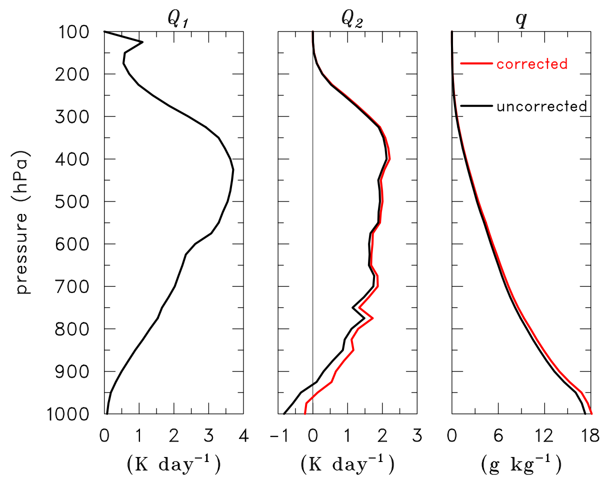

Figure 8: IFA-IOP mean vertical profiles of apparent heating (left), apparent drying (middle) and specific humidity (right) computed with humidity corrected (red curve) and uncorrected (black curve) data.

Table 2 shows the impact of using the HC data on the IFA-IOP means of the budget-derived quantities. Using the HC data increases the mean rainfall estimate by 6% to 8.4 mm day^{-1}, while the mean net-radiative heating decreases by 38% to -0.55 K day^{-1}. These radiative estimates include an additional cooling of 0.05 K day^{-1} due to the effects of rain on the computation of ω, the sensible heat flux due to rain, and the frictional dissipation associated with falling rain (Johnson and Ciesielski 2000). The small differences (0.3 mm day^{-1} and 0.03 K day^{-1} for rainfall and net-radiation, respectively) between the uncorrected estimates listed in Table 3 and the corresponding values cited in Johnson and Ciesielski (2000) are due to the spurious divergence correction (Haertel 2002) used in the present study. These revised values based on HC data agree well with other independent estimates of these quantities shown in Table 2.

Separating the radiative estimates for periods with clear and cloudy conditions, we find that during clear sky conditions (defined here as period when the IFA-mean GMS-4 brightness temperatures was greater than 5°C which occurs about 35% of the time) $\Delta < Q_R >$ is -0.01 K day^{-1}. For the remaining periods, that is, with cloudy conditions, $\Delta < Q_R >$ is -0.23 K day^{-1}. In analyzing the radiative impact of the humidity corrected data at R/V *Moana Wave*, Guichard et al. found that with clear sky conditions use of the HC data in their radiative model produces an additional net cooling of 1.29 W

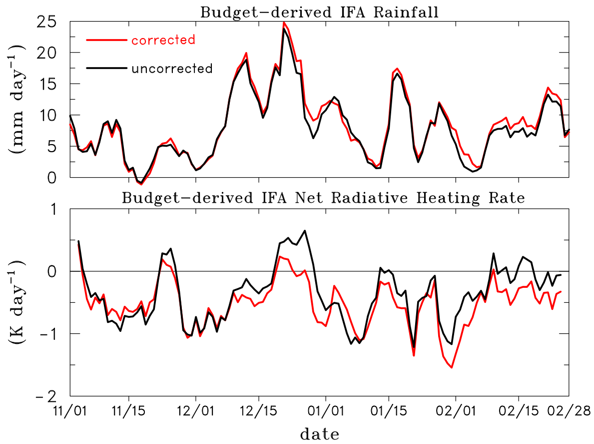

Figure 9: Time series of IFA-mean rainfall (top panel) and net-radiative heating (bottom panel) diagnosed from the atmospheric budget with corrected humidity (red curve) and uncorrected (black curve) data for the COARE IOP.

	P (mm day^{-1})	$<Q_R>$ (K day^{-1})
uncorrected	7.90	−0.40
change (Δ)	0.50 (+6%)	−0.15 (−38%)
corrected	8.40	−0.55
independent estimates	8.3 (Curry et al. 1999) 9.3 (CMAP)	−0.38 (B. Collins, cited in Wu et al. 2000) −0.66 (C. Long, cited in Jensen et al. 2002) −0.79 (Rossow-Zhang, based on Curry et al. 1999)

Table 2. Impact of corrected humidity data on IFA-IOP means of budget-derived quantities.

m^{-2} (or −0.012 K day^{-1})[6] which agrees well with our clear sky estimate. However under cloudy conditions, their model produces an additional net cooling of 1.07 W m^{-2} (or −0.01 K day^{-1}) due to the HC data which is considerably less than our estimate of −0.23 K day^{-1}. It is difficult to understand the reasons for this difference, since the methods (budget residual versus direct radiative computation) are so different. One reason for this difference may be that the radiative computation of Guichard et al. (2000) did not consider any changes in cloud cover when using humidity corrected or uncorrected data. They acknowledge that such cloud cover changes would significantly impact their radiative computations. While beyond the scope of this study, it would be interesting to examine the radiative impact of the HC data within the context of a complete atmospheric model with interactive radiation.

[6]This assumes 108 W m^{-2} = −1.1 K day^{-1}.

Revised estimates with HC data of rainfall and net-radiative heating rates for the Outer Sounding Array (OSA) are 8.9 mm day^{-1} and −0.62 K day^{-1} for the IOP-means, respectively, compared to previous estimates of 9.3 mm day^{-1} and −0.50 K day^{-1} (Johnson and Ciesielski 2000). Sensitivity tests show that the changes in the OSA estimates are due predominately to the spurious divergence correction (Haertel 2002). For this larger area the low-level drying in the corrected VIZ data has a compensating effect on the budget quantities relative to the moistening effects of the corrected Vaisala data.

6. IMPACT ON FORCING FIELDS FOR CRMS AND SCMS

Yet another method for assessing the impact of the HC data is through a moist enthalpy analysis. CRMs and SCMs are forced with large-scale advective tendencies of temperature (f_T) and moisture (f_q) given by

$$f_T = -(c_{pd} + c_l q)[\mathbf{v} \cdot \nabla T + \omega(\partial T/\partial p) - \alpha\omega]$$

$$f_q = -[\mathbf{v} \cdot \nabla q + \omega(\partial q/\partial p)]$$

where c_{pd} is the specific heat capacity for dry air and c_l is the specific heat capacity of liquid water. Predicted enthalpy K_p is a function of these forcing tendencies (Wu et al. 2000), which typically are computed from gridded objective analysis averaged over a given region. If observed enthalpy $K_o = (c_{pd} + c_l q)T + Lq$ differs significantly from K_p, then CRM and SCM simulations will develop temperature and moisture biases. Emanuel and Živković-Rothman (1999) and Wu et al. (2000) have performed a moist enthalpy analysis for the TOGA COARE period to evaluate the quality of the large-scale forcing data. The large-scale forcing data they used were computed from an objective analysis scheme similar to what is used in this study but with no correction for spurious divergence or humidity (Ciesielski et al. 1997). Their analysis at the end of a 120-day integration for COARE IOP showed differences between observed and predicted enthalpy "equivalent to a 25 K temperature error integrated over the troposphere" (Emanuel and Živković-Rothman 1999).

Following the procedure outlined in Wu et al. (2000) and using his radiative flux data, we repeat this moist enthalpy analysis. Figure 10 shows the observed and predicted enthalpy (computed both with and without HC data) for the COARE IOP.

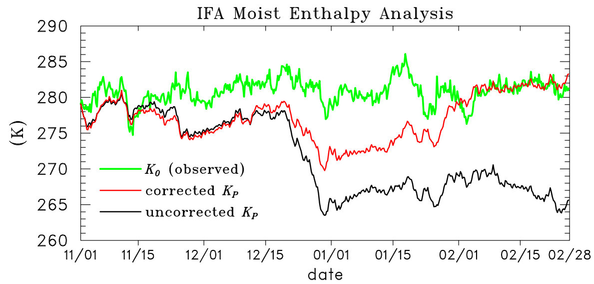

Figure 10: Evolution of the IFA-mean 6-hourly observed moist enthalpy (green curve) and the predicted enthalpy computed with humidity corrected (red curve) and uncorrected (black curve) data. Following the convention of Wu et al. (2000), observed enthalpy is divided by c_{pd} and predicted enthalpy is divided by $c_{pd} \times 958$ hPa.

At the end of the 120-day integration the difference between K_p and K_o with uncorrected humidity data is about 15 K; with HC data the difference is only a few degrees [7]. This suggests that a model simulation of the entire IOP forced with the HC data would exhibit less of an enthalpy trend than one forced with the uncorrected data.

7. IMPACT ON THE DIURNAL CYCLE

Wang et al. (2002) noted that four island VaH sites (Kapinga, Kavieng, Manus and Nauru) have a significantly larger correction during the daytime. While the reasons for this day-night difference are still being investigated, we consider here how the corrected humidities affect the diurnal cycle over the IFA. The change in specific humidity (Δq) in the boundary layer due to the HC data is shown in the top panel of Fig. 11. As noted by Wang et al. a larger increase in moisture occurs during the daylight hours (10 and 16LT). Above the boundary layer, no significant diurnal variation in Δq is observed.

With positive Δq at all hours one might also expect an increased rainfall and decreased in $<Q_R>$ at all hours. Instead, the change in the diurnal variation of these fields is more complex. A significant rainfall increase and $<Q_R>$ decrease is observed at 16 and 22 LT with a weaker but opposite trend at 04 and 10LT (bottom two panels of Fig. 11). The primary reason for this result is due to the the local tendency term ($\partial q/\partial t$) which is generally small in

[7] The spurious divergence correction largely accounts for the smaller 120-day entropy trend of 15 K compared to the 25 K found by Emanuel and Živković-Rothman (1999) and Wu et al. (2000).

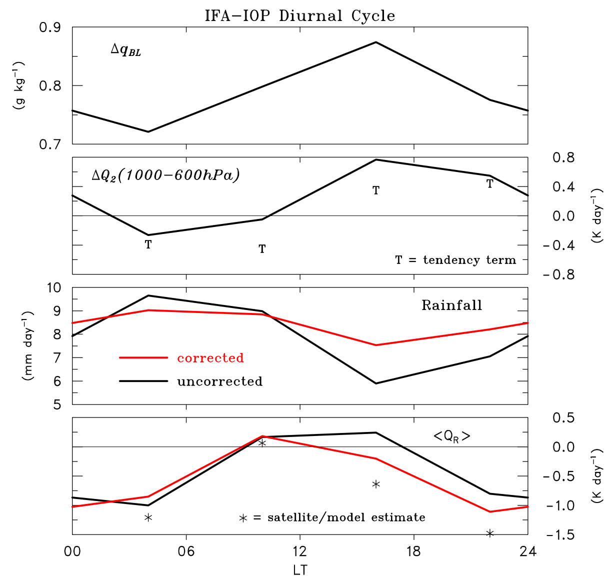

Figure 11: Diurnal cycle of IFA-IOP mean fields. Change in boundary layer specific humidity (Δq_{bl}) due to the humidity correction (top panel), change in lower-tropospheric (1000-600 hPa) apparent drying (ΔQ_2) due to the humidity correction (second panel) where the 'T' symbols show the contribution to ΔQ_2 due to the tendency term, budget-derived rainfall computed with humidity corrected (red curve) and uncorrected (black curve) data (third panel), budget-derived net-radiative heating computed with humidity corrected (red curve) and uncorrected (black curve) data (bottom panel). Also denoted by the star symbols ($*$) in the bottom panel are satellite/model estimates of net-radiative heating from W. Rossow and Y.-C. Zhang (personal communication, based on Curry et al. 1999).

magnitude compared to the vertical advection term, but on diurnal time scale can significantly impact the moisture budget. In this case the effect of local tendency term (indicated with the "T" symbols in the second panel of Fig. 11) has a moistening effect at 04 and 10LT and drying effect at 16 and 22LT. Also shown here is the resulting change in the Q_2 field (ΔQ_2) due to the HC data. Given this diurnal variation of ΔQ_2 and the direct proportionality of $<Q_2>$ to P and $-<Q_R>$ in budget equations (2) and (3), one can readily see how the HC data impacts changes in rainfall and net-radiative heating (bottom two panels of Fig. 11, respectively).

The main impact of using the HC data is a reduction in the amplitude of the diurnal rainfall variation by increasing the rainfall amount at 16 and 22 LT. With the caveat that resolving diurnal features with 6-hourly observations is difficult and results inconclusive, we offer the following comparisons with other studies. The early morning maximum in budget-derived rainfall is consistent with radar analysis of Short et al. (1997) which covered a region about half the size of the IFA and was available for 101 days of the 120 day IOP. Their radar analysis also showed a 10 LT minimum in rainfall and a secondary afternoon maximum. While the afternoon increase in rainfall computed with the HC data may be an improvement in terms of capturing the afternoon secondary maximum observed by radar, the 6-hourly budget analysis is unable to resolve neither this maximum precisely nor the 10 LT rainfall minimum detected by the radar. Use of the HC data increases the net-radiative cooling rate at 16 and 22 LT with little impact at other hours, resulting in a diurnal variation in better agreement with an independent estimate (denoted by the $*$ symbols in Fig. 11) provided by W. Rossow and Y.-C. Zhang (personal communication, based on Curry et al. 1999). The impact is particularly large at 16 LT where the uncorrected data show a net warming of 0.24 K day^{-1}, while the corrected data show a net cooling of -0.20 K day^{-1} .

8. SUMMARY AND CONCLUSIONS

This study investigates the impacts of the humidity-corrected (HC) dataset, released by NCAR/ATD, on various analyses over the LSA domain of COARE. The dataset contains corrected humidity for 42 sounding sites in the COARE domain which includes both Vaisala and VIZ systems. The nature of the Vaisala humidity errors, which come from six sources, is discussed in detail in Wang et al. (2002). This study describes the correction procedure for the VIZ humidity errors. The humidity corrections, which are largest in the lower tropospheric levels, generally increase the moisture in the Vaisala sondes and decrease it in the VIZ sondes.

Because of the sensitivity of convection to low-level thermodynamic properties, use of the HC data gives one a much different perspective on the characteristics of convection during TOGA COARE. For example, the moisture increase in the HC VaH sondes, launched primarily from sites in the IFA, increases the IOP-mean value of CAPE by 450 J kg^{-1} and decreases the CIN by 96 J kg^{-1}. Opposite trends in these parameters are observed at the VIZ sites which lie along the northern edge of the LSA. With uncorrected data, the difference in the IOP-mean CAPE between the VaH and VIZ sites is over 700 J kg^{-1}; after correction both CAPEs are $\sim$1250 J kg^{-1}, which is consisent with a generally uniform SST field over the warm pool.

Application of the HC data to a 1-D cloud model shows that convective mass fluxes in the 500-300 hPa layer increase $\sim$30% for the VaH sites near the equator and decrease $\sim$15% at the VIZ sites near 10°N. These results suggest that the intensity and location of convection would be significantly different in model simulations which use the HC data. Using uncorrected data one might mistakenly conclude that convection is difficult to trigger over the IFA and overly-primed for vigorous convection at the VIZ sites to the north. Use of the HC data gives a more realistic view of the atmosphere's convective potential and its spatial distribution over warm pool region. In addition, we have noted the difficulty that the reanalysis products had in reproducing the rainfall pattern observed during COARE – a likely consequence of the humidity instrument biases. For this reason, we believe that the reanalysis products for the COARE period could be improved with a new reanalysis using the corrected humidity data.

Use of the HC data appears to have a beneficial impact on budget-derived estimates. The IFA-IOP mean rainfall diagnosed as budget residual increases by 6% (from 7.9 to 8.4 mm day^{-1}) due to the HC data. A more substantial change is observed in the IFA-IOP mean of net-radiative heating which decreases by 38% (from -0.40 to -0.55 K day^{-1}) from using the HC data. These new estimates based on the HC data are in better agreement with those from other independent sources.

We also examined the impact of the HC data in terms of a moist enthalpy analysis. Such analysis has been used by previous investigators to evaluate the quality of the large-scale forcing data for CRM and SCM simulations. Our analysis suggests that model simulations of the entire IOP forced with HC data will exhibit substantially smaller enthalpy trends than simulations forced with uncorrected data.

The efforts invested to correct the sonde humidity data have gone a long way towards improving the quality of the humidity field for COARE. Unfortunately some errors still remain. The most notable problems in the HC dataset that we are aware of include: (1) a significant moist bias in the R/V *Kexue 1* sonde data still exist and appears to have gotten worse in the "corrected" dataset, (2) the original humidity data from the R/V *Vickers* is judged to be of good quality, whereas the correction scheme appears to dry the sondes too much, (3) use of the R/V *Moana Wave* humidity data in a study of the mixed layer over the warm pool suggests that it may have been slightly under corrected (i.e., not moistened enough), and (4) no corrections have been made to the VIZ sondes above 700 hPa. Despite these lingering issues, the improvements already made to the TOGA COARE upper-air sonde dataset make it one of the highest quality tropical sonde datasets ever collected.

Based on the comparison of several analyses with and without the humidity corrections, we contend that the HC dataset described herein has resulted in a much improved large-scale analysis of the water-vapor field for the COARE IOP. These improvements should lead to more accurate simulations of convection and large-scale circulations in global models, as well as, in CRMs and SCMs. To encourage the use of this improved dataset, our gridded LSA analyses and large-scale forcing dataset computed with the HC data, as described in this paper, have been made available at

ACKNOWLEDGMENTS This research has been supported by the NOAA Project NA67RJ0152. Thanks go to Junhong Wang for her help with the VIZ corrections, and to Pat Haertel for comments on the manuscript. We commend the efforts of Ed Zipser whose persistence in calling attention to the humidity errors in the TOGA COARE sonde data ultimately lead to their correction. Thanks also go to Paquita Zuidema and Brian Mapes for providing us with the code for the buoyancy-sorting cloud model and for their patience in helping us use it, to Xiaoqing Wu for furnishing us with the radiative flux data used in the moist enthalpy analysis, to Yuanchong Zhang and Bill Rossow for making available their latest radiative estimates for the COARE period, and for the assistance of Rick Taft in developing the code for the multiquadric interpolation scheme.

9. REFERENCES

Ciesielski, P. E., L. M. Hartten, and R. H. Johnson, 1997: Impacts of merging profiler and rawinsonde winds on TOGA COARE analyses. *J. Atmos. Oceanic. Technol.*, **14**, 1264–1279.

Curry, J. A., C. A. Clayson, W. B. Rossow, R. Reeder, Y.-C. Zhang, P. J. Webster, G. Liu, and R.-S. Sheu, 1999: High resolution satellite derived data set of the surface fluxes of heat, freshwater, and momentum for the TOGA-COARE IOP. *Bull. Amer. Meteor. Soc.*, **80**, 2059–2080.

Emanuel, K. A., and M. Živković-Rothman, 1999: Development and evaluation of a convection scheme for use in climate models. *J. Atmos. Sci.*, **56**, 1766–1782.

Ferrier, B. S., and R. A. Houze Jr., 1989: One-dimensional time dependent modeling of GATE cumulonimbus convection. *J. Atmos. Sci.*, **46**, 330–351.

Gallus, W. A., Jr., and R. H. Johnson, 1991: Heat and moisture budgets of an intense midlatitude squall line. *J. Atmos. Sci.*, **48**, 122–146.

Guichard, F., D. Parsons, and E. Miller, 2000: Thermodynamic and radiative impact of the correction of sounding humidity bias in the Tropics. *J. Climate*, **13**, 3611–3624.

Haertel, P. T., 2002: Spurious divergence within objective analyses with application to TOGA COARE heat and moisture budgets. *Preprints, 25th Conference on Hurricanes and Tropical Meteorology*, Amer. Meteor. Soc., San Diego, CA, 192–195.

Johnson, R. H., P. E. Ciesielski, and K. A. Hart, 1996: Tropical inversions near the 0° level. *J. Atmos. Sci.*, **53**, 1838–1855.

Johnson, R. H., and P. E. Ciesielski, 2000: Rainfall and radiative heating rate estimates from TOGA-COARE atmospheric budgets. *J. Atmos. Sci.*, **57**, 1497–1514.

Johnson, R. H., P. E. Ciesielski, and J. A. Dickey, 2001: Multiscale variability of the atmospheric mixed layer over the Western Pacific warm pool. *J. Atmos. Sci.*, **58**, 2729–2750.

Johnson, R. H., P. E. Ciesielski, and B. E. Mapes, 2002: Effects of random sampling errors on TOGA-COARE atmospheric budgets. *Preprints, 25th Conference on Hurricanes and Tropical Meteorology*, Amer. Meteor. Soc., San Diego, CA, 194–195.

LeMone, M. E. Zipser, and S. Trier, 1998: The role of environmental shear and thermodynamic conditions in determining the structure and evolution of mesoscale convective systems during TOGA COARE. *J. Atmos. Sci.*, **55**, 3493–3518.

Lin, X., and R. H. Johnson, 1996: Heating, moistening and rainfall over the western Pacific warm pool during TOGA COARE. *J. Atmos. Sci.*, **53**, 3367-3383.

Lucas, C., and E. J. Zipser, 2000: Environmental variability during TOGA COARE. *J. Atmos. Sci.*, **57**, 2333–2350.

Lucas, C., E. J. Zipser, and B. S. Ferrier, 2000: Sensitivity of tropical west Pacific oceanic squall lines to tropospheric wind and moisture profiles. *J. Atmos. Sci.*, **57**, 2351–2373.

Nuss, W. A., and D. W. Titley, 1994: Use of multiquadric interpolation for meteorological objective analysis. *Mon. Wea. Rev.*, **122**, 1611–1631.

Ooyama, K., 1987: Scale-controlled objective analysis. *Mon. Wea. Rev.*, **115**, 2476–2506.

Raymond, D. J., A. M. Blyth, 1992: Extensions of the stochastic mixing model to cumulonimbus clouds. *J. Atmos. Sci.*, **49**, 1968–1983.

Short, D. A., P. A. Kucera, B. S. Ferrier, J. C. Gerlach, S. A. Rutledge, and O. W. Thiele, 1997: Shipboard radar rainfall patterns within the TOGA COARE IFA. *Bull. Amer. Meteor. Soc.*, **78**, 2817–2836.

Wade, C. G., and B. Schwartz, 1993: Radionsonde humidity observations near saturation. Preprints, *Eight Symp. on Meteorological Observations and Instrumentation*, Anaheim, CA, Amer. Meteor. Soc., 44–49.

Wang, J., H. L. Cole, D. J. Carlson, E. R. Miller, K. Beierle, A. Paukkunen, and T. K. Laine, 2002: Corrections of humidity measurement errors from the Vaisala RS80 radiosonde – Application to TOGA-COARE data. *J. Atmos. Oceanic. Technol.*, **19**, 981–1002.

Webster, P. J., and R. Lukas, 1992: TOGA COARE: The Coupled Ocean-Atmosphere Response Experiment. *Bull. Amer. Meteor. Soc.*, **73**, 1377–1416.

Wu, X., M. W. Moncrieff, and K. A. Emanuel, 2000: Evaluation of large-scale forcing during TOGA COARE for cloud-resolving models and single-column models. *J. Atmos. Sci.*, **57**, 2977–2985.

Xie, P., and P. A. Arkin, 1997: Global precipitation: A 17-year monthly analysis based on gauge observations, satellite estimates, and numerical model output. *Bull. Amer. Meteor. Soc.*, **78**, 2539–2558.

Yanai, M., S. Esbensen, and J. H. Chu, 1973: Determination of bulk properties of tropical cloud clusters from large-scale heat and moisture budgets. *J. Atmos. Sci.*, **30**, 611–627.

Zhang, M. H., and J. L. Lin, 1997: Constrained variational analysis of sounding data based on column-integrated conservations of mass, heat, moisture, and momentum: Approach and application to ARM measurements. *J. Atmos. Sci.*, **54**, 1503–1524.

Zipser, E. J., and R. H. Johnson, 1998: Systematic errors in radiosonde humidities: A global problem? *Preprints, 10th Symposium on Meteorological Observations and Instrumentation*, Amer. Meteor. Soc., Phoenix, 72–73.

Zuidema, P., 1998: The 600–800-mb minimum in tropical cloudiness observed during TOGA COARE. *J. Atmos. Sci.*, **55**, 2220–2228.